

Structure and dynamics of interfaces between two coexisting liquid-crystalline phases

Simon Praetorius,¹ Axel Voigt,¹ Raphael Wittkowski,² and Hartmut Löwen³

¹*Institute of Scientific Computing, Technical University Dresden, D-01062 Dresden, Germany*

²*SUPA, School of Physics and Astronomy, University of Edinburgh, Edinburgh, EH9 3JZ, United Kingdom*

³*Institut für Theoretische Physik II, Weiche Materie, Heinrich-Heine-Universität Düsseldorf, D-40225 Düsseldorf, Germany*

(Received 1 February 2013; published 28 May 2013)

A phase-field-crystal model is used to access the structure and thermodynamics of interfaces between two coexisting liquid-crystalline phases in two spatial dimensions. Depending on the model parameters, there is a variety of possible coexistences between two liquid-crystalline phases, including a plastic triangular crystal (PTC). Here, we numerically calculate the profiles for the mean density and for the nematic order tensor across the interface for isotropic-PTC and columnar-PTC (or equivalently smectic-*A*-PTC) phase coexistence. As a general finding, the width of the interface with respect to the nematic order parameter characterizing the orientational order is larger than the width of the mean-density interface. In approaching the interface from the PTC side, at first, the mean density goes down, and then the nematic order parameter follows. The relative shift in the two profiles can be larger than a full lattice constant of the plastic crystal. Finally, we also present numerical results for the dynamic relaxation of an initial order-parameter profile towards its equilibrium interfacial profile. Our predictions for the interfacial profiles can, in principle, be verified in real-space experiments of colloidal dispersions.

DOI: [10.1103/PhysRevE.87.052406](https://doi.org/10.1103/PhysRevE.87.052406)

PACS number(s): 68.08.De, 61.30.Dk, 64.70.D-, 82.70.Dd

I. INTRODUCTION

Liquid crystals, typically composed of anisometric molecules or colloidal particles, form interesting mesophases, which are neither completely liquid nor completely crystalline [1]. The simultaneous presence of translational and rotational degrees of freedom gives rise to phases which exhibit a different degree of ordering for the translational and orientational orders [2,3]. Rotator solids or plastic crystals, for instance, are translationally ordered but orientationally disordered, whereas nematics, on the other hand, possess orientational order in the absence of translational order. Clearly, there also are the fully disordered isotropic phase and the fully ordered crystalline phase, but there are even more intermediate liquid-crystalline phases (such as, for example, smectic-*A* and columnar phases) with different degrees of translational and orientational orders that are stable for appropriate thermodynamic conditions.

It is a formidable task of statistical physics to predict the existence and stability of the different liquid-crystalline phases for a given interaction as a function of mean density and temperature. This has, for example, been performed by computer simulations of simple model systems [4,5] and by molecular density functional theory [6,7] and more phenomenological approaches [8]. Typically, phase diagrams of liquid crystals exhibit regions where two phases of different kinds of ordering coexist. At equal pressure, chemical potential, and temperature, coexistence implies that there is a stable interface between the two coexisting phases. In mean-field theories (which neglect interfacial capillary wave undulations), the interface has a characteristic width of typically several particle sizes and exhibits profiles of the mean density and of the degree of orientational order depending on the spatial coordinate perpendicular to the interface. For the liquid-solid interface, see, for example, Refs. [9–14].

Although there has been a large effort to explore the gas-liquid [15] and liquid-solid [16] interfaces of spherical particles (see also Refs. [17–23]), much less effort has been devoted to the particle-resolved structure and thermo-

dynamics of the interface between two coexisting *liquid-crystalline* phases. Extensive studies have been performed for the isotropic-nematic interface, which has been accessed by experiment, computer simulation, and theory (see, for example, Refs. [24–32]), but there are fewer considerations of the isotropic-smectic [33–36] and the nematic-smectic interfaces [37]. Therefore, we investigate an interface where one of the coexisting phases is plastic or fully crystalline here. This is, of course, a nontrivial task since there is a complex dependence of the interface structure on the (relative) orientation of the two phases. Even for the isotropic-crystal coexistence, there is a complex orientational dependence culminating in Wulff’s construction for the equilibrium crystal shape [23]. Nevertheless, it is important to have information about the interface since nucleation and growth phenomena of a metastable phase in a stable phase occur via interfaces [36,38,39].

In this paper, we close this gap and study liquid-crystalline interfaces for crystalline phases. We use a phase-field-crystal (PFC) model, which is a minimal model to describe freezing for isotropic particles on the molecular (i.e., interparticle) scale [40–42] and can be justified from microscopic density functional theory [42–44]. The traditional PFC model [40] was later generalized to anisotropic particles in two [45] and three [46] spatial dimensions allowing for liquid-crystalline phases. The generalized theory is formulated in terms of three order-parameter fields, namely, the reduced translational density $\psi(\vec{r})$, the local nematic order parameter $S(\vec{r})$, and the mean orientational direction $\hat{n}(\vec{r})$ that is also called the “nematic director.” Whereas the traditional PFC model [40] has two free parameters, the liquid-crystalline PFC model in two dimensions [45] has five independent couplings. This widely opens the parameter space for the occurrence of several liquid-crystalline phases including nematic, columnar, smectic-*A*, plastic-crystalline, and orientationally ordered crystalline phases. Recent numerical studies [47] of the liquid-crystalline PFC model in two spatial dimensions have shown that a variety of phase coexistences occur as a function of

the model parameters. Therefore, the liquid-crystalline PFC model [45] provides a simple and direct avenue to access the interface structure, which still incorporates the correct physics.

As a result, we find that the width of the interface with respect to the nematic order parameter is larger than the width of the mean-density interface. In approaching the interface from the plastic-crystalline side, at first, the mean density goes down, and then the nematic order parameter follows. The relative shift in these two profiles can be larger than a full lattice constant of the plastic crystal. Finally, we also present numerical results for the dynamic relaxation of an initial order-parameter profile towards its equilibrium interfacial profile. Our results can, in principle, be verified in real-space experiments of colloidal dispersions, which can be confined to monolayers [48–51]. A transient nonmonotonic behavior of the conserved mean-density profiles occurs, which is much more pronounced than nonmonotonicities in the nonconserved orientational-order profile.

The paper is organized as follows: after the presentation of a suitable PFC model for liquid crystals in Sec. II, we discuss results obtained by numerical calculations in Sec. III. We finally conclude in Sec. IV.

II. PFC MODEL FOR LIQUID CRYSTALS IN TWO SPATIAL DIMENSIONS

A PFC model for apolar¹ liquid crystals in two spatial dimensions was given in Refs. [42,45,47,52,53]. It describes the static properties and dynamical behavior of a liquid-crystalline system in terms of two dimensionless order-parameter fields: the reduced translational density $\psi(\vec{r}, t)$ and the symmetric and traceless nematic tensor $Q_{ij}(\vec{r}, t)$ with position $\vec{r} = (x, y)$ and time t . For liquid-crystalline particles with a symmetry axis, the nematic tensor can be parametrized as

$$Q_{ij}(\vec{r}, t) = S(\vec{r}, t)(n_i(\vec{r}, t)n_j(\vec{r}, t) - \frac{1}{2}\delta_{ij}), \quad (1)$$

with the nematic order parameter $S(\vec{r}, t)$ and the (normalized) nematic director $\hat{n}(\vec{r}, t) = (n_1, n_2)$ (see Refs. [45,47,52]).

A. Static free-energy functional

The static properties of a liquid-crystalline system are described by a free-energy functional $\mathcal{F}[\psi, Q_{ij}]$, which is minimized with respect to $\psi(\vec{r})$ and $Q_{ij}(\vec{r})$ in thermodynamic equilibrium. After an appropriate rescaling of the length and energy scales, this free-energy functional obtains the dimensionless form² [53]

$$\begin{aligned} \mathcal{F}[\psi, Q_{ij}] = \int d^2r \left(-\frac{\psi^3}{3} + \frac{\psi^4}{6} + (\psi - 1)\frac{\psi Q_{kl}^2}{4} \right. \\ \left. + \frac{Q_{kl}^2 Q_{mn}^2}{64} + A_1 \psi^2 + A_2 \psi(\Delta + \Delta^2)\psi \right. \\ \left. + B_3(\partial_k \psi)(\partial_l Q_{kl}) + D_1 Q_{kl}^2 + D_2(\partial_l Q_{kl})^2 \right), \end{aligned} \quad (2)$$

¹We neglect a possible macroscopic polarization.

²Einstein's sum convention is used throughout this paper. Notice that powers of indexed quantities involve repeated indices and, thus, summation, i.e., for example, $Q_{ij}^2 \equiv Q_{ij}Q_{ij} \equiv \sum_{i,j} Q_{ij}Q_{ij}$.

with the Laplace operator $\Delta \equiv \partial_k^2$ and the five dimensionless coupling parameters A_1 , A_2 , B_3 , D_1 , and D_2 .

B. Dynamical equations

The corresponding dynamical equations of $\psi(\vec{r}, t)$ and $Q_{ij}(\vec{r}, t)$ can be derived from classical dynamical density functional theory [54] and are given by [53]

$$\dot{\psi} + \partial_i J_i^\psi = 0, \quad (3)$$

$$\dot{Q}_{ij} + \Phi_{ij}^Q = 0, \quad (4)$$

with the dimensionless current $J_i^\psi(\vec{r}, t)$ and the dimensionless quasicurrent $\Phi_{ij}^Q(\vec{r}, t)$. In constant-mobility approximation, this current and quasicurrent are given by [42]

$$J_i^\psi = -2\alpha_1(\partial_i \psi^\natural) - 2\alpha_3(\partial_j Q_{ij}^\natural), \quad (5)$$

$$\Phi_{ij}^Q = -4\alpha_1(\Delta Q_{ij}^\natural) - 2\alpha_3[2(\partial_i \partial_j \psi^\natural) - \delta_{ij}(\Delta \psi^\natural)] + 8\alpha_4 Q_{ij}^\natural, \quad (6)$$

with the three dimensionless mobility parameters α_1 , α_3 , and α_4 and the thermodynamic conjugates,

$$\psi^\natural = \frac{\delta \mathcal{F}}{\delta \psi}, \quad Q_{ij}^\natural = \frac{\delta \mathcal{F}}{\delta Q_{ij}}, \quad (7)$$

of $\psi(\vec{r}, t)$ and $Q_{ij}(\vec{r}, t)$, respectively. The thermodynamic conjugates follow directly from the free-energy functional (2) by functional differentiation:

$$\begin{aligned} \psi^\natural = -\psi^2 + \frac{2}{3}\psi^3 + (2\psi - 1)\frac{Q_{ij}^2}{4} + 2A_1\psi \\ + 2A_2(\Delta + \Delta^2)\psi - B_3(\partial_i \partial_j Q_{ij}), \end{aligned} \quad (8)$$

$$\begin{aligned} Q_{ij}^\natural = \psi(\psi - 1)Q_{ij} + \frac{Q_{ij}Q_{kl}^2}{8} \\ - B_3[2(\partial_i \partial_j \psi) - \delta_{ij}\Delta\psi] + 4D_1Q_{ij} \\ - 2D_2\partial_k[\partial_i Q_{kj} + \partial_j Q_{ki} - \delta_{ij}(\partial_l Q_{kl})]. \end{aligned} \quad (9)$$

For a comparison of the dimensionless rescaled parameters in Eqs. (2), (5), and (6) with the corresponding parameters in the notation of Refs. [42,47,53], see Appendix A. The numerical procedure to solve the system of equations is briefly described in Appendix B.

III. RESULTS

We first restrict ourselves to certain parameter combinations, which allow for several liquid-crystalline coexistences. In detail, we fix parameters $A_2 = 14$, $B_3 = -0.4$, $D_1 = 1$, and $D_2 = 0.8$ but vary parameter A_1 (which corresponds to some formal temperature in the context of mean-field theories) and the reduced mean density $\bar{\psi}$.³ The resulting equilibrium bulk phase diagram is shown in Fig. 1 in consistency with earlier data [47]. In the parameter range of A_1 and $\bar{\psi}$ shown, the phase diagram exhibits three stable liquid-crystalline phases,

³The parameters in the dynamical equations (3)–(6) are always chosen to be $\alpha_1 = \alpha_3 = \alpha_4 = 1$. Clearly, the stationary results do not depend on their particular values.

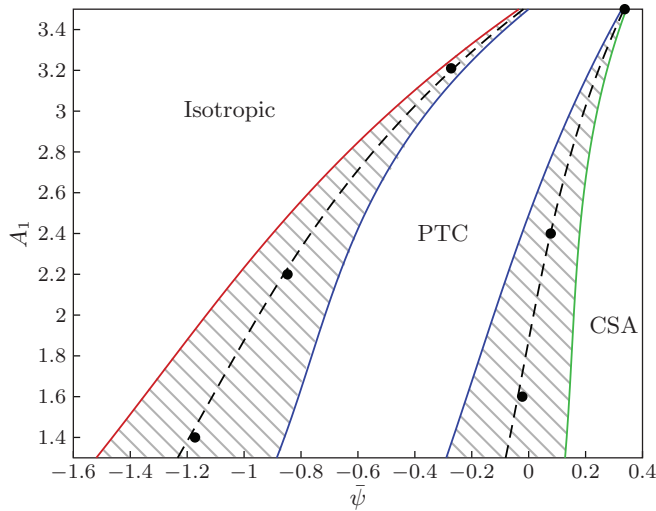


FIG. 1. (Color online) Phase diagram with coexistence regions for the mean density $\bar{\psi} \in [-1.6, 0.4]$ and parameters $A_1 \in [1.3, 3.5]$, $A_2 = 14$, $B_3 = -0.4$, $D_1 = 1$, and $D_2 = 0.8$. Three different liquid-crystalline phases are realized: isotropic, columnar or smectic- A (CSA), and PTC. The coexistence regions (shaded areas) are calculated using Maxwell’s double tangent construction. The black dashed lines in the coexistence regions indicate the intersection lines of the energy curves of the two adjacent phases. Six black circles indicate certain parameter combinations for which detailed calculations were performed (see Figs. 3–8).

namely, the isotropic phase, a PTC,⁴ and a columnar phase. As we consider two spatial dimensions here, a columnar phase is indistinguishable from a smectic- A phase, therefore, we call the latter the CSA⁵ phase. The coexistence regions, as obtained by a Maxwell double tangent construction, are depicted by the shaded area in Fig. 1. We selected, in total, six different coexistence conditions as labeled by black circles in Fig. 1, which correspond to three isotropic-PTC and three CSA-PTC coexistence situations serving as basic reference situations for our subsequent investigations.

A typical example for an isotropic-PTC interfacial profile is presented in Fig. 2 for the (10) orientation of the hexagonal crystal.⁶ In the bulk PTC phase, there are periodic peaks in the full density profile $\psi(x, y)$ at the crystal lattice positions, shown as a contour plot in Fig. 2. The typical standard deviation of these peaks (the so-called Lindemann parameter) is pretty large with about 27% of the lattice constant. The corresponding orientational ordering, as embodied in the nematic tensor, is complicated and exhibits topological defects in the Wigner-Seitz cell of the lattice, see Refs. [47,55] for more detailed discussions. The mean orientational unit vector

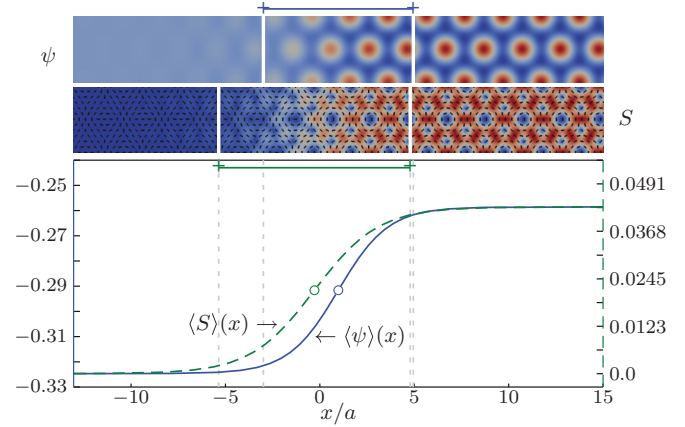


FIG. 2. (Color online) Top: two contour plots for $\psi(x, y)$ and $S(x, y)$ at an isotropic-PTC coexistence with $A_1 = 3.21$ and $\bar{\psi} = -0.3$ (the other parameters are the same as in Fig. 1). $\hat{n}(\vec{r})$ is represented by short black lines that are superimposed on the lower contour plot. Bottom: left ordinate: averaged density $\langle \psi \rangle(x)$ and right ordinate: averaged nematic order parameter $\langle S \rangle(x)$. The x direction is chosen perpendicular to the interface, whereas, the y axis is parallel to the interface. The averaged quantities are defined by $\langle f \rangle(x) = \int dy' \int_{x-a}^{x+a} dx' f(x', y')$ for $f \in \{\psi, S\}$ with the width of the stripes $2a = 4\pi/(k\sqrt{3})$ and $k = 1/\sqrt{2}$.

field $\hat{n}(x, y)$, as obtained by the direction of the eigenvector of the nematic tensor corresponding to the highest eigenvalue, is sketched by short black lines in Fig. 2. The largest eigenvalue itself multiplied by 2—the scalar nematic order-parameter field $S(x, y)$ —is also presented as a contour plot in Fig. 2. In the isotropic phase, on the other hand, the density field is constant, and the nematic order parameter vanishes. In between, there is an interfacial region with laterally averaged profiles $\langle \psi \rangle(x)$ and $\langle S \rangle(x)$ with x denoting the direction perpendicular to the interface (see the caption for Fig. 2).

We define a typical interface width of an order-parameter profile $f(x, y) \in \{\psi(x, y), S(x, y)\}$ as the distance of the positions where a hyperbolic-tangent approximation of $\langle f \rangle(x)$ attains the values $0.95\langle f \rangle(-\infty) + 0.05\langle f \rangle(\infty)$ and $0.05\langle f \rangle(-\infty) + 0.95\langle f \rangle(\infty)$, respectively. These widths for $\psi(x, y)$ and $S(x, y)$ are indicated in Fig. 2. Remarkably, the width of the density profile is significantly smaller than the width of the orientational profile. The position where the hyperbolic-tangent approximation of an averaged field $\langle f \rangle(x)$ with $f \in \{\psi, S\}$ attains the value $[\langle f \rangle(-\infty) + \langle f \rangle(\infty)]/2$ can be taken as a natural location $\xi(f)$ of the interface with respect to this field. Interestingly, as revealed in Fig. 2, the location of the averaged density profile $\langle \psi \rangle(x)$ and the averaged orientational profile $\langle S \rangle(x)$ do not coincide. The location of the orientational profile is more shifted towards the isotropic phase than the location of the density profile. This means that, coming from the isotropic side, at first, the nematic order builds up and then the density follows. This finding is reminiscent of the fluid-crystal interface of systems of spherical particles [23,56], which can be described by a two-order-parameter description involving the conserved mean density and a nonconserved crystallinity [11,57]. Coming from the fluid side, also in this case, the nonconserved crystallinity starts to grow first, and the density follows.

⁴The plastic triangular crystal in Fig. 1 is called the “plastic triangular crystal 2” in Ref. [47].

⁵This CSA phase is called the “C/SA phase” in Ref. [47].

⁶In our calculations, the one-mode approximation was used to determine the lattice spacing in the y direction. In fact, we found, for varied periodicity in the y direction, that the free-energy density is minimal for a lattice spacing very close to the one-mode approximation such that the system is practically not strained in the y direction.

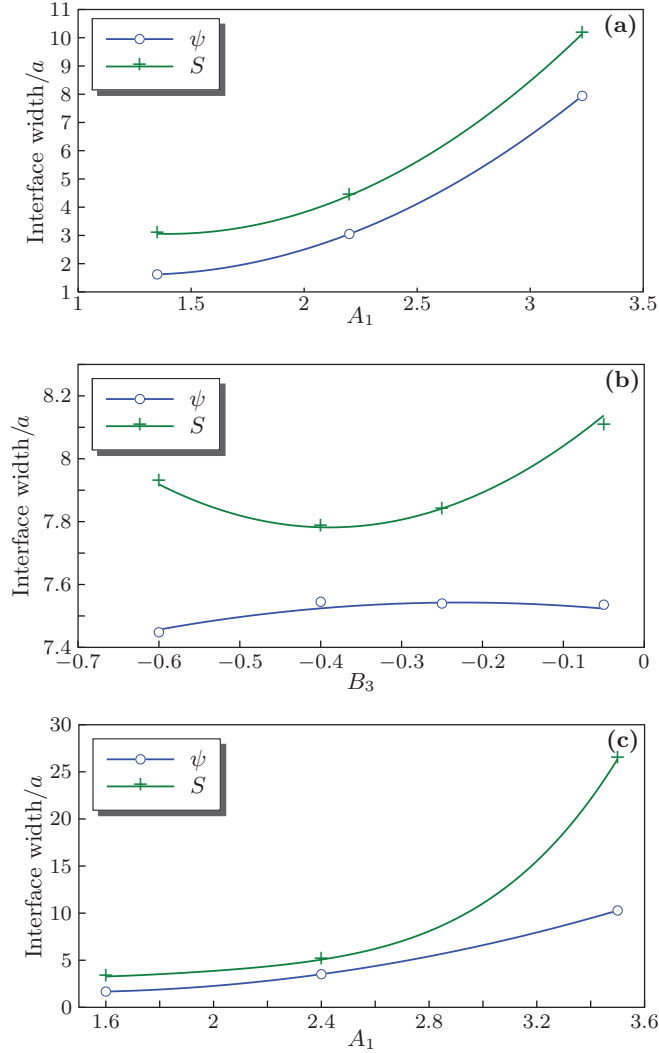


FIG. 3. (Color online) Widths of the (a), (b) isotropic-PTC, and the (c) CSA-PTC interfaces of $\psi(\vec{r})$ and $S(\vec{r})$ in dependence on A_1 and B_3 , respectively. The parameters are (a) $(\bar{\psi}, A_1) \in \{(-1.2, 1.3), (-0.85, 2.2), (-0.3, 3.21)\}$, (b) $B_3 \in \{-0.6, -0.4, -0.25, -0.05\}$ with fixed $(\bar{\psi}, A_1) = (-0.3, 3.21)$, and (c) $(\bar{\psi}, A_1) \in \{(-0.05, 1.6), (0.05, 2.4), (0.31, 3.5)\}$ where the remaining parameters are as in Fig. 1. Notice that the presented data in (a) and (c) correspond to the six points highlighted by the black circles in Fig. 1 and that they are connected by polynomial fitting curves. In (c), the stripes of the CSA phase are oriented perpendicular to the interface (see Fig. 5).

We have further studied the dependence of the interface widths on parameters A_1 and B_3 . As A_1 is increased, the coexistence comes closer to a critical point where the interfacial widths diverge. This trend is documented in Fig. 3(a). Figure 3(a) also shows that the width of the orientational-order-parameter profile is larger than that of the density interface over the full range of A_1 . All trends are the same for different parameter combinations for the isotropic-PTC interface as documented by Fig. 4. The dependence of the interface width on parameter B_3 as shown in Fig. 3(b) is much less pronounced than the dependence on parameter A_1 . Interestingly, the interface width of the orientational-order-parameter profile is again larger than the width of the density

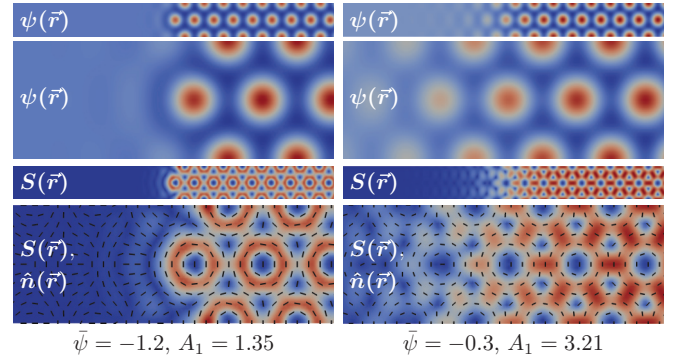


FIG. 4. (Color online) Interface of the isotropic-PTC phase coexistence for the same parameters as in Fig. 1. The plots show the translational density $\psi(\vec{r})$ and the nematic order parameter $S(\vec{r})$ both for a large area and for a closeup view of the interface where blue (gray) and red (dark gray) indicate low and high values, respectively. In addition, the director field $\hat{n}(\vec{r})$ is represented by short black lines that are superimposed on the lowest plots.

interface. The trend of the curves indicates that this behavior also holds for a larger parameter interval of B_3 than plotted in Fig. 3(b). However, due to the huge parameter space and high computational complexity of the calculations, we cannot rule out the possibility that there is a certain combination of the five parameters of the PFC model where the interface width for the orientational-order-parameter profile is not larger than for the density profile.

Next, we consider the coexistence between the PTC and the CSA phases. In this case, the interface structure depends on the relative orientations of the two phases. While we fix the orientation of the PTC phase in the (10) direction, here, we consider two different possibilities of the column direction relative to the interface, namely, perpendicular and parallel. For these two relative orientations, the order-parameter fields are given in Figs. 5 and 6 for two different parameter combinations of coexistence.⁷ For the perpendicular column direction (see Fig. 5), the density field reveals that the columns end at a lattice density peak. This implies that the degeneracy of the column positions is broken by the presence of the crystal, which pins the transversal columnar order by the interface. Along the columns away from the interface, there are still some density undulations in the x direction. For the parallel column direction (see Fig. 6), on the other hand, there is a nontrivial density field across the interface insofar as the columns are significantly bent in the presence of the crystalline peaks, i.e., the crystal induces a systematic undulation of the neighboring columns. The amplitude of this undulation decreases farther away from the interface position. Likewise, along the columns, there is a

⁷It is important to note that, in Fig. 5, the interface connects two phases which have, in principle, different periodicities in the y direction. Therefore, care has to be taken in determining the box size in the y direction, in particular, if these two periodicities are incommensurate. We have checked that a doubled system size in the y direction does not affect the results. Nevertheless, a much larger system size could possibly lead to superstructures which are not explored in the present paper.

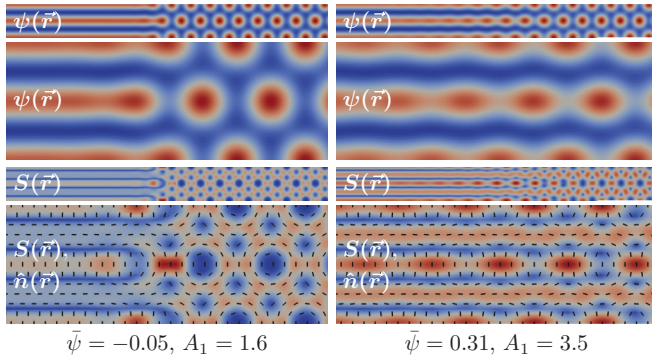


FIG. 5. (Color online) The same as in Fig. 4 but, now, for the CSA-PTC interface. Note that the stripes of the CSA phase are oriented perpendicular to the interface.

periodic density modulation in the y direction induced by the crystalline peaks nearby.

Results for the interfacial widths, similarly defined as in the previous case, are shown in Fig. 3(c) where the same trends are observed as for the isotropic-PTC interface [see Fig. 3(a)]. The width of the orientational interface is considerably larger than that for the density profile, and there is a strong dependence on parameter A_1 with huge interfacial widths where the parameter is close to criticality. Both for the isotropic-PTC coexistence and for the CSA-PTC coexistence, the interface position of the density profile is more shifted towards the PTC phase than the interface position of the orientational profile, which is more in the coexisting CSA phase (see Fig. 7). As shown in Fig. 7, the distance of the two interface positions depends on parameters A_1 and B_3 .

Finally, we show some results on the dynamical evolution of the interfacial profiles based on the physical dynamics described by Eqs. (3) and (4). It is important to note that the density is a conserved order parameter, whereas, the nematic ordering is nonconserved. We plotted an example of the interface relaxation towards equilibrium for a prescribed starting profile in Fig. 8. The orientational-order-parameter field is a smeared Heaviside step function, whereas, the density is constant. Similar setups for interfacial kinetics have been

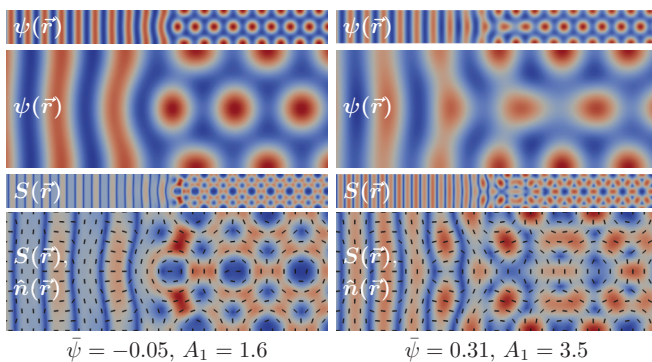


FIG. 6. (Color online) The same as in Fig. 5 but, now, for a CSA-PTC interface where the stripes of the CSA phase are oriented parallel to the interface.

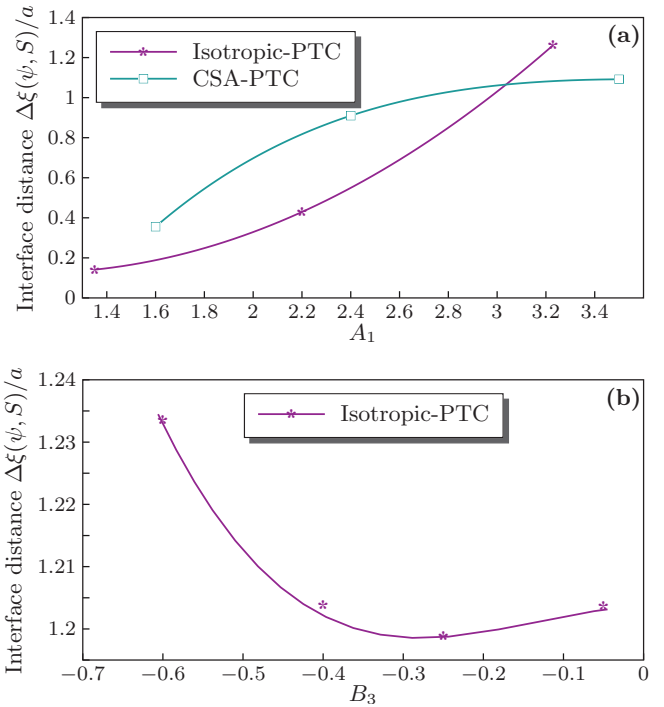


FIG. 7. (Color online) Distance $\Delta\xi(\psi, S) = \xi(\psi) - \xi(S)$ of the interfaces of $\psi(\vec{r})$ and $S(\vec{r})$ in dependence on (a) A_1 and (b) B_3 where we always consider the transition from the noncrystalline to the crystalline phase. The parameters are the same as in Fig. 3, and the stripes of the CSA phase are, again, oriented perpendicular to the interface (see Fig. 5).

studied earlier [58]. The density field, subsequently, takes up the orientational inhomogeneity, and both order parameters relax to their equilibrium profiles. The density develops a marked transient nonmonotonic profile and relaxes much slower than the orientational order. It takes quite a long time in units of the basic time scale of the dimensionless dynamical equations (3)–(6) to end up in the final equilibrium state. These findings show that our dynamical equations (3) and (4), which reflect the diffusive dynamics of colloidal systems, can, in principle, be applied to plenty of further growth phenomena in the future, which are, however, beyond the scope of the present paper.

IV. CONCLUSIONS

In conclusion, we have explored the equilibrium structure of interfaces between various coexisting liquid-crystalline phases using a PFC model for liquid crystals. In two spatial dimensions, we have considered explicitly the isotropic-plastic-crystalline and the smectic-A-plastic-crystalline interfaces, which are both anisotropic, i.e., they depend on the relative orientation of the two coexisting phases. To determine the equilibrium structures numerically, we calculated the relaxation of the dissipative PFC dynamics towards equilibrium (i.e., the minimization of the PFC functional) under the constant-mobility approximation using the finite element method.

Basically, we have considered a two-order-parameter description of the interfaces containing the conserved

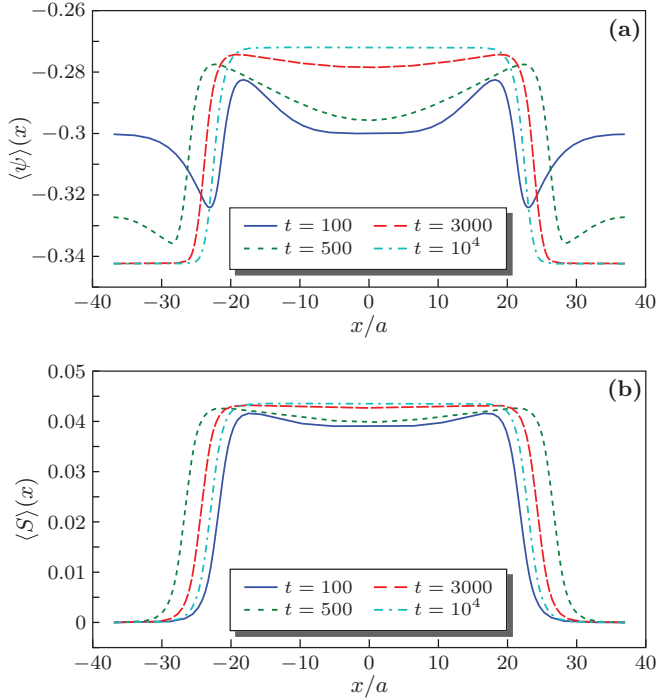


FIG. 8. (Color online) Time evolution of the averaged order parameters (a) $\langle\psi\rangle(x)$ and (b) $\langle S\rangle(x)$ for an isotropic-PTC coexistence. The parameters are $\alpha_1 = \alpha_3 = \alpha_4 = 1$, $\bar{\psi} = -0.3$, $A_1 = 3.21$, and for the rest, as in Fig. 1. Snapshots are taken at times $t = 100, 500, 3000$, and $10\,000$. At time $t = 0$, the averaged translational density is constant ($\langle\psi\rangle(x) = -0.3$), and the averaged nematic order parameter $\langle S\rangle(x)$ is a smeared Heaviside step function.

(translational) density field and the nonconserved (orientational) nematic tensor. The phase diagram, the typical widths of the interfaces, the order-parameter profiles, and their dynamics were computed. For the isotropic-plastic-crystalline interface, we found that, in approaching the interface from the isotropic side, at first, the nematic order builds up and then the density follows. The relative shift in the two profiles is about half the lattice constant of the plastic crystal. This finding is reminiscent of the fluid-crystal interface of systems of spherical particles [23,56], which can be described by a two-order-parameter description involving the conserved mean density and a nonconserved crystallinity [11,57]. For the fluid-crystal interface, a similar shift has been found: If the interface is approached from the fluid side, first, the (nonconserved) crystallinity increases, and then the (conserved) mean density follows [11,59–61]. This has to do with the fact that a fluid is more responsive to an oscillatory density wave than to a global density change [59]. For the smectic-*A*-plastic-crystalline interface, we found a similar behavior as for the isotropic-plastic-crystalline interface with a shift in the density interface towards the plastic-crystalline phase. Furthermore, our results show that, in the whole parameter range we explored, the width of the interface with respect to the nematic order parameter is larger than the width of the mean-density interface.

Our results can be verified either in particle-resolved computer simulations [62] or in experiments. Particle-resolved computer simulations for rodlike systems have been performed

both for structure [4,63–65] and for dynamics [66,67] in various situations. So far as experiments are concerned, most notably, colloidal liquid crystals [3,68,69] that are confined to two spatial dimensions are the ideal realizations of our model. One important example is a suspension of the tobacco mosaic virus, which can be confined to monolayers [50] and which shows a variety of liquid-crystalline phases [8], but there are many other examples of liquid-crystalline rodlike particle suspensions, which have been prepared in a controlled way (see, e.g., Refs. [48,49,51]).

Future work should extend the present study to three spatial dimensions [42,46], which would require more numerical work but promises a richer equilibrium bulk phase diagram. Also, the dynamics of a growing crystalline front, which already has been studied in detail for spherical particles [70–72], should be addressed for liquid crystals as well. If a plastic-crystalline phase grows into an isotropic phase, it would be interesting to follow the origin of topological defects in the director field, which have to grow out of nothing. Moreover, crystal-fluid interfaces in external fields, such as gravity, already exhibit unusual effects for isotropic particles [73,74], and it would be challenging to explore this for liquid-crystalline interfaces [75]. Finally, our model should be generalized towards liquid crystals on manifolds [76] to describe nematic [77] or smectic bubbles [78].

ACKNOWLEDGMENTS

We thank R. Backofen for helpful discussions. R.W. gratefully acknowledges financial support from a Postdoctoral Research Fellowship (Grant No. WI 4170/1-1) of the German Research Foundation (DFG). In addition, this work was supported by the DFG within SPP 1296.

APPENDIX A: NOTATION

Since the PFC model presented in Sec. II is equivalent to PFC models given in different notations in Refs. [42,47,53], here, we clarify the relationship of our notation to the notation used in the literature. This especially simplifies the comparison of Fig. 1 to the corresponding phase diagrams in Ref. [47].

If we denote the eight parameters in Eqs. (2), (5), and (6) with a prime (i.e., $A'_1, A'_2, B'_3, D'_1, D'_2, \alpha'_1, \alpha'_3$, and α'_4) to avoid confusion with similar notations in Refs. [42,53], the characteristic length l'_c and the characteristic energy E'_c , which have been chosen to make the PFC model in the present article dimensionless, can be expressed by $l'_c = \sqrt{-A_3/A_2}$ and $E'_c = -(\pi\bar{\rho}/\beta)(A_3/A_2)$ in terms of the reference particle number density $\bar{\rho}$, the inverse thermal energy β , and parameters A_2 and A_3 in Ref. [53]. In Ref. [42], the notation is analogous but with ρ_{ref} instead of $\bar{\rho}$.

The parameters in the free-energy functional (2) can be related to the parameters in Refs. [42,53] by

$$A'_1 = 1 - \frac{A_1}{2\pi\bar{\rho}}, \quad A'_2 = -\frac{A_2^2}{2\pi\bar{\rho}A_3}, \quad B'_3 = \frac{A_2B_3}{2\pi\bar{\rho}A_3}, \quad (\text{A1})$$

and

$$D'_1 = \frac{1}{4} - \frac{D_1}{2\pi\bar{\rho}}, \quad D'_2 = \frac{A_2D_2}{2\pi\bar{\rho}A_3}. \quad (\text{A2})$$

In the case of the current (5) and the quasicurrent (6), a comparison with Refs. [42,53] leads to the relations

$$\alpha'_1 = \frac{t_c E_c}{l_c^2} \alpha_1, \quad \alpha'_3 = \frac{t_c E_c}{l_c^2} \alpha_3, \quad \alpha'_4 = t_c E_c \alpha_4. \quad (\text{A3})$$

In Ref. [47], a different notation is used. A comparison of the free-energy functional (2) with the corresponding free-energy functional in Ref. [47] leads to

$$A'_1 = B_l, \quad A'_2 = 4B_x, \quad B'_3 = -4F, \quad (\text{A4})$$

and

$$D'_1 = 2D, \quad D'_2 = 8E. \quad (\text{A5})$$

Furthermore, the length and energy scales of these two free-energy functionals are different. If l'_c and E'_c denote the characteristic length and energy in the present article and l_c and E_c denote the corresponding quantities in Ref. [47], they can be related to each other by

$$l'_c = \frac{1}{\sqrt{2}} l_c, \quad E'_c = \frac{1}{2} E_c. \quad (\text{A6})$$

APPENDIX B: NUMERICAL SOLUTION OF THE PFC MODEL

By inserting Eqs. (8) and (9) into Eqs. (5) and (6), one obtains for the dynamical equations (3) and (4) a system of six coupled nonlinear partial differential equations. In order to solve this system numerically, we decoupled and linearized it. A simplification is possible due to the symmetry and tracelessness of the nematic tensor. Defining variables $q_i \equiv Q_{i,1}$ and $q_i^\natural \equiv Q_{i,1}^\natural$ allows us to write the system of dynamical equations in the compact form

$$\begin{aligned} \dot{\psi} &= 2\alpha_1 \Delta \psi^\natural + 2\alpha_3 \blacktriangle_i q_i^\natural, \\ \dot{q}_i &= 4\alpha_1 \Delta q_i^\natural + 2\alpha_3 \blacktriangle_i \psi^\natural - 8\alpha_4 q_i^\natural, \end{aligned} \quad (\text{B1})$$

with the operator $\blacktriangle \equiv (\partial_1 \partial_1 - \partial_2 \partial_2, 2\partial_1 \partial_2)$, that is related to the Cauchy-Riemann operator. The thermodynamic conjugates

reformulated in the new variables read

$$\begin{aligned} \psi^\natural &= \omega_\psi(\psi, \vec{q}) + 2A_1 \psi + 2A_2 (\Delta + \Delta^2) \psi - B_3 \blacktriangle_i q_i, \\ q_i^\natural &= \omega_q(\psi, \vec{q})_i + 4D_1 q_i - 2D_2 \Delta q_i - B_3 \blacktriangle_i \psi, \end{aligned} \quad (\text{B2})$$

with the polynomials

$$\begin{aligned} \omega_\psi(\psi, \vec{q}) &= -\psi^2 + \frac{2}{3} \psi^3 + \frac{1}{2} (2\psi - 1) q_i^2, \\ \omega_q(\psi, \vec{q})_i &= \psi(\psi - 1) q_i + \frac{1}{4} q_i q_j^2. \end{aligned} \quad (\text{B3})$$

To discretize the dynamical equations (B1) in time, let t_1, t_2, t_3, \dots be a sequence of time steps. Defining $\psi_n \equiv \psi(\vec{r}, t_n)$, $q_{i,n} \equiv q_i(\vec{r}, t_n)$, and $\tau_n = t_{n+1} - t_n$, we obtain (by an operator-splitting approach) the decoupled systems

$$\begin{aligned} \frac{\psi_{n+1}}{\tau_n} - 2\alpha_1 \Delta \psi_{n+1}^\natural &= \frac{\psi_n}{\tau_n} + 2\alpha_3 \blacktriangle_i q_{i,n}^\natural, \\ \psi_{n+1}^\natural - 2[A_1 - A_2 (\Delta + \Delta^2)] \psi_{n+1} & \\ &= \omega_\psi(\psi_{n+1}, \vec{q}_n) - B_3 \blacktriangle_i q_{i,n} \end{aligned} \quad (\text{B4})$$

and

$$\frac{q_{i,n+1}}{\tau_n} - 4(\alpha_1 \Delta - 2\alpha_4) q_{i,n+1}^\natural = \frac{q_{i,n}}{\tau_n} + 2\alpha_3 \blacktriangle_i \psi_n^\natural, \quad (\text{B5})$$

$$q_{i,n+1}^\natural - 2(2D_1 - D_2 \Delta) q_{i,n+1} = \omega_q(\psi_n, \vec{q}_{n+1})_i - B_3 \blacktriangle_i \psi_n.$$

Linearizing $\omega_\psi(\psi, \vec{q})$ and $\omega_q(\psi, \vec{q})_i$ around the old time step t_n , two linear systems can be solved one after the other for all n . The linearizations of the polynomials (B3) read

$$\begin{aligned} \omega_\psi(\psi_{n+1}, \vec{q}_n) &\approx \psi_{n+1} (-2\psi_n + 2\psi_n^2 + q_{i,n}^2) \\ &\quad + \psi_n^2 - \frac{4}{3} \psi_n^3 - \frac{q_{i,n}^2}{2}, \\ \omega_q(\psi_n, \vec{q}_{n+1})_i &\approx \frac{1}{4} q_{i,n+1} [4\psi_n (\psi_n - 1) + q_{j,n}^2] \\ &\quad + \frac{1}{2} q_{i,n} q_{j,n} q_{j,n+1} - \frac{1}{2} q_{i,n} q_{j,n}^2. \end{aligned} \quad (\text{B6})$$

Instead of such a simple time-stepping scheme, we used a higher-order embedded Rosenbrock scheme (see, for example, Refs. [79,80]) with an adequate step-size control for the time discretization. A detailed description of this scheme concerning some numerical issues will be given elsewhere. For the discretization in space, we used the finite element method.

-
- [1] P.-G. de Gennes and J. Prost, *The Physics of Liquid Crystals*, 2nd ed., International Series of Monographs on Physics Vol. 83 (Oxford University Press, Oxford, 1995).
- [2] D. Frenkel, in *Liquids, Freezing and Glass Transition, Proceedings of the Les Houches Summer School, Course LI, 3-28 July 1989*, edited by J.-P. Hansen, D. Levesque, and J. Zinn-Justin (North-Holland, Elsevier Science B. V., Amsterdam, 1991), Vol. 2, p. 689.
- [3] G. J. Vroege and H. N. W. Lekkerkerker, *Rep. Prog. Phys.* **55**, 1241 (1992).
- [4] P. Bolhuis and D. Frenkel, *J. Chem. Phys.* **106**, 666 (1997).
- [5] J. T. Brown, M. P. Allen, E. Martín del Río, and E. de Miguel, *Phys. Rev. E* **57**, 6685 (1998).
- [6] A. Poniewierski and R. Hołyst, *Phys. Rev. Lett.* **61**, 2461 (1988).
- [7] H. Graf and H. Löwen, *J. Phys.: Condens. Matter* **11**, 1435 (1999).
- [8] H. Graf and H. Löwen, *Phys. Rev. E* **59**, 1932 (1999).
- [9] W. A. Curtin, *Phys. Rev. Lett.* **59**, 1228 (1987).
- [10] W. A. Curtin, *Phys. Rev. B* **39**, 6775 (1989).
- [11] H. Löwen, T. Beier, and H. Wagner, *Europhys. Lett.* **9**, 791 (1989).
- [12] R. Ohnesorge, H. Löwen, and H. Wagner, *Phys. Rev. A* **43**, 2870 (1991).
- [13] D. W. Marr and A. P. Gast, *Phys. Rev. E* **47**, 1212 (1993).
- [14] R. Ohnesorge, H. Löwen, and H. Wagner, *Phys. Rev. E* **50**, 4801 (1994).
- [15] R. Evans, *Adv. Phys.* **28**, 143 (1979).

- [16] D. P. Woodruff, *The Solid-Liquid Interface*, 1st ed., Cambridge Solid State Science Series Vol. 1 (Cambridge University Press, London, 1980).
- [17] K. Binder and M. Müller, *Int. J. Mod. Phys. C* **11**, 1093 (2000).
- [18] J. J. Hoyt, M. Asta, and A. Karma, *Phys. Rev. Lett.* **86**, 5530 (2001).
- [19] R. L. Davidchack, J. R. Morris, and B. B. Laird, *J. Chem. Phys.* **125**, 094710 (2006).
- [20] T. Zykova-Timan, R. E. Rozas, J. Horbach, and K. Binder, *J. Phys.: Condens. Matter* **21**, 464102 (2009).
- [21] T. Zykova-Timan, J. Horbach, and K. Binder, *J. Chem. Phys.* **133**, 014705 (2010).
- [22] R. E. Rozas and J. Horbach, *Europhys. Lett.* **93**, 26006 (2011).
- [23] A. Härtel, M. Oettel, R. E. Rozas, S. U. Egelhaaf, J. Horbach, and H. Löwen, *Phys. Rev. Lett.* **108**, 226101 (2012).
- [24] A. J. McDonald, M. P. Allen, and F. Schmid, *Phys. Rev. E* **63**, 010701(R) (2000).
- [25] E. Velasco, L. Mederos, and D. E. Sullivan, *Phys. Rev. E* **66**, 021708 (2002).
- [26] M. Bier, L. Harnau, and S. Dietrich, *Phys. Rev. E* **69**, 021506 (2004).
- [27] R. L. C. Vink and T. Schilling, *Phys. Rev. E* **71**, 051716 (2005).
- [28] D. van der Beek, H. Reich, P. van der Schoot, M. Dijkstra, T. Schilling, R. Vink, M. Schmidt, R. van Roij, and H. Lekkerkerker, *Phys. Rev. Lett.* **97**, 087801 (2006).
- [29] S. Wolfsheimer, C. Tanase, K. Shundyak, R. van Roij, and T. Schilling, *Phys. Rev. E* **73**, 061703 (2006).
- [30] H. Reich, M. Dijkstra, R. van Roij, and M. Schmidt, *J. Phys. Chem. B* **111**, 7825 (2007).
- [31] B. Ullrich, G. K. Auernhammer, E. M. Sam, and D. Vollmer, *Colloids Surf. A* **354**, 298 (2010).
- [32] A. A. Verhoeff, R. H. J. Otten, P. van der Schoot, and H. N. W. Lekkerkerker, *J. Chem. Phys.* **134**, 044904 (2011).
- [33] L. Mederos and D. E. Sullivan, *Phys. Rev. A* **46**, 7700 (1992).
- [34] A. M. Somoza, L. Mederos, and D. E. Sullivan, *Phys. Rev. E* **52**, 5017 (1995).
- [35] C. Blanc, *Phys. Rev. E* **64**, 011702 (2001).
- [36] Z. Dogic and S. Fraden, *Philos. Trans. R. Soc. London, Ser. A* **359**, 997 (2001).
- [37] M. A. Osipov, J. R. Sambles, and L. Ruan, *Liq. Cryst.* **30**, 823 (2003).
- [38] T. Schilling and D. Frenkel, *Phys. Rev. Lett.* **92**, 085505 (2004).
- [39] A. A. Verhoeff and H. N. W. Lekkerkerker, *Soft Matter* **8**, 4865 (2012).
- [40] K. R. Elder, M. Katakowski, M. Haataja, and M. Grant, *Phys. Rev. Lett.* **88**, 245701 (2002).
- [41] A. Jaatinen and T. Ala-Nissila, *J. Phys.: Condens. Matter* **22**, 205402 (2010).
- [42] H. Emmerich, H. Löwen, R. Wittkowski, T. Gruhn, G. I. Tóth, G. Tegze, and L. Gránásy, *Adv. Phys.* **61**, 665 (2012).
- [43] K. R. Elder, N. Provatas, J. Berry, P. Stefanovic, and M. Grant, *Phys. Rev. B* **75**, 064107 (2007).
- [44] S. van Teeffelen, R. Backofen, A. Voigt, and H. Löwen, *Phys. Rev. E* **79**, 051404 (2009).
- [45] H. Löwen, *J. Phys.: Condens. Matter* **22**, 364105 (2010).
- [46] R. Wittkowski, H. Löwen, and H. R. Brand, *Phys. Rev. E* **82**, 031708 (2010).
- [47] C. V. Achim, R. Wittkowski, and H. Löwen, *Phys. Rev. E* **83**, 061712 (2011).
- [48] S. Roorda, T. van Dillen, A. Polman, C. Graf, A. van Blaaderen, and B. J. Kooi, *Adv. Mater.* **16**, 235 (2004).
- [49] A. Turković, P. Dubček, and N. D. Fox, *Vacuum* **80**, 108 (2005).
- [50] S. P. Wargacki, B. Pate, and R. A. Vaia, *Langmuir* **24**, 5439 (2008).
- [51] J. J. Crassous, H. Dietsch, P. Pfeleiderer, V. Malik, A. Diaz, L. A. Hirshi, M. Drechsler, and P. Schurtenberger, *Soft Matter* **8**, 3538 (2012).
- [52] R. Wittkowski, H. Löwen, and H. R. Brand, *Phys. Rev. E* **83**, 061706 (2011).
- [53] R. Wittkowski, H. Löwen, and H. R. Brand, *Phys. Rev. E* **84**, 041708 (2011).
- [54] R. Wittkowski and H. Löwen, *Mol. Phys.* **109**, 2935 (2011).
- [55] P. Cremer, M. Marechal, and H. Löwen, *Europhys. Lett.* **99**, 38005 (2012).
- [56] J. F. Lutsko, *Advances in Chemical Physics*, 1st ed. (Wiley, Hoboken, NJ, 2010), Vol. 144, p. 1.
- [57] H. Löwen, T. Beier, and H. Wagner, *Z. Phys. B: Condens. Matter* **79**, 109 (1990).
- [58] H. Löwen and D. W. Oxtoby, *J. Chem. Phys.* **93**, 674 (1990).
- [59] H. Löwen and T. Beier, *Phys. Rev. B* **41**, 4435 (1990).
- [60] M. Oettel, S. Dorosz, M. Berghoff, B. Nestler, and T. Schilling, *Phys. Rev. E* **86**, 021404 (2012).
- [61] M. Oettel, *J. Phys.: Condens. Matter* **24**, 464124 (2012).
- [62] A. V. Ivlev, H. Löwen, G. E. Morfill, and C. P. Royall, *Complex Plasmas and Colloidal Dispersions: Particle-Resolved Studies of Classical Liquids and Solids*, 1st ed., Series in Soft Condensed Matter Vol. 5 (World Scientific, Singapore, 2012).
- [63] D. J. Cleaver, C. M. Care, M. P. Allen, and M. P. Neal, *Phys. Rev. E* **54**, 559 (1996).
- [64] N. Akino, F. Schmid, and M. P. Allen, *Phys. Rev. E* **63**, 041706 (2001).
- [65] M. Marechal and M. Dijkstra, *Phys. Rev. E* **77**, 061405 (2008).
- [66] H. Löwen, *Phys. Rev. E* **50**, 1232 (1994).
- [67] T. Kirchhoff, H. Löwen, and R. Klein, *Phys. Rev. E* **53**, 5011 (1996).
- [68] Z. Dogic and S. Fraden, *Phys. Rev. Lett.* **78**, 2417 (1997).
- [69] M. P. Lettinga, J. K. G. Dhont, Z. Zhang, S. Messlinger, and G. Gompper, *Soft Matter* **6**, 4556 (2010).
- [70] K. Sandomirski, E. Allahyarov, H. Löwen, and S. Egelhaaf, *Soft Matter* **7**, 8050 (2011).
- [71] G. Tegze, G. I. Tóth, and L. Gránásy, *Phys. Rev. Lett.* **106**, 195502 (2011).
- [72] M. J. Robbins, A. J. Archer, U. Thiele, and E. Knobloch, *Phys. Rev. E* **85**, 061408 (2012).
- [73] T. Biben, R. Ohnesorge, and H. Löwen, *Europhys. Lett.* **28**, 665 (1994).
- [74] E. Allahyarov and H. Löwen, *Europhys. Lett.* **95**, 38004 (2011).
- [75] M. Marechal and M. Dijkstra, *Soft Matter* **7**, 1397 (2011).
- [76] I. Nitschke, A. Voigt, and J. Wensch, *J. Fluid Mech.* **708**, 418 (2012).
- [77] J. Dzubiella, M. Schmidt, and H. Löwen, *Phys. Rev. E* **62**, 5081 (2000).
- [78] K. May, K. Harth, T. Trittel, and R. Stannarius, *Europhys. Lett.* **100**, 16003 (2012).
- [79] J. Lang, *Adaptive Multilevel Solution of Nonlinear Parabolic PDE Systems: Theory, Algorithm, and Applications*, 1st ed., Lecture Notes in Computational Science and Engineering Vol. 16 (Springer-Verlag, Berlin, 2000).
- [80] J. Rang and L. Angermann, *BIT Numer. Math.* **45**, 761 (2005).